Influence of Ti and Co/Ni Ratio on the Oxidation at 1200 °C of Chromium-Containing {Ni, Co}-Based Cast Alloys

PATRICE BERTHOD and SYNTHIA ANNICK OZOUAKI WORA

This work investigates the possible influence that titanium may have on the oxidation of {nickel and/or cobalt}-based chromium-rich alloys. It starts with the elaboration by casting of a series of alloys from pure elements, with a base element ranging from nickel only to cobalt only. To magnify these possible effects of titanium and reach the atomic equivalence with the carbon present (0.4 wt pct C) in the alloys, 1.6 wt pct Ti was introduced in the chemical composition. To amplify the oxidation process, the oxidation tests carried out in laboratory air were run at the constant temperature of 1200 °C for a rather long time (170 hours). The surface states and cross-sections were characterized by XRD, electron microscopy and EDS analyses. The results demonstrate that all the alloys (except the nickel-free cobalt-based one) resisted oxidation rather well without catastrophic evolution due to titanium. The tested Ti content led to significant internal oxidation and to an external selective oxidation producing a thin layer stick on the outer side of the chromia scale. It is supposed that this outermost TiO_2 layer may be beneficial for the oxidation behavior by the possible limitation of the deleterious over-consumption of chromium by chromia re-oxidation/volatilization. This will be later verified by further investigations combining thermogravimetry follow-up of the oxidation rate and analysis of chromium balance sheets.

https://doi.org/10.1007/s11661-021-06519-8

I. INTRODUCTION

NICKEL and cobalt-based superalloys are designed to be refractory enough to be used at elevated temperature as well as to efficiently resist both chemical and mechanical constrains in service, notably hot oxidation and creep deformation.[1,2] The presence of aluminum and/or chromium in enough quantity favors the development of an external continuous oxide scale protecting the alloy while the introduction of other elements allows obtaining high mechanical properties at high temperature. This mechanical resistance can be achieved by solid solution strengthening or by the precipitation of reinforcing particles. Some of these elements introduced for alloy strengthening purpose may be themselves involved in the hot oxidation process and therefore, by their presence, they may influence the general oxidation progress affecting the alloy, with possible deleterious consequences for the sustainability of the concerned components. This is particularly true in the case of elements more oxidizable than the metal(s) chosen for obtaining the protective external oxide scale (aluminum or chromium).[3,4] Titanium is one of these very reactive elements able to take part to oxidation in parallel with aluminum and chromium, and thus to influence the oxidation behavior of the whole alloy.

Titanium can be found notably in some nickel-based superalloys.[5] For example, it is—beside aluminum—one of the constituents of the gamma prime precipitates of some single crystals.[5,6] Titanium can be also met in superalloys based on nickel and cobalt simultaneously,[7] in recent cast cobalt alloys,[8] and even in some single crystalline cobalt-based superalloys.[9]

Titanium is also often encountered in superalloys as TiC carbides. Conventionally cast nickel-based alloys are particularly concerned,[10,11] but also nickel-based single crystals,[12,13] coatings and composites.[14,15] Titanium monocarbides are of the same carbides family as TaC or HfC. When they form in significant quantity in conventionally cast superalloys during their solidification, they may appear at the end of solidification as eutectic carbides with a Chinese script shape. This particular morphology, observed for instance in polycrystalline equi-axed chromium-rich cobalt-based superalloys,[16] was identified as potentially very beneficial for

PATRICE BERTHOD is with the Université de Lorraine, CNRS, IJL, Campus Artem, Postal Box 50840, 54000 Nancy, France and also with the Université de Lorraine, FST, Campus Victor Grignard, Postal Box 70239, 54500 Vandoeuvre-lès-Nancy, France. Contact e-mail: patrice.berthod@univ-lorraine.fr SYNTHIA ANNICK OZOUAKI WORA is with the Université de Lorraine, FST.

Manuscript submitted August 20, 2021; accepted October 25, 2021. Article published online November 12, 2021

the strength at elevated temperature. Indeed TaC also presents this morphology in creep-resistant Co(Ni)-based industrial superalloys[17–19] and in Fe-based alloys.[20,21] This can be also said for HfC recently obtained in significant quantity in Co-based[22] and Ni-based[23] academic alloys. The carbides of titanium have the advantage of a lower density by comparison with the ones of the other monocarbides which involve much heavier metallic elements such as Ta or Hf, with as consequence a slight lowering of the volume mass of the whole alloy.

In the present study, the influence of 1.6 wt pct Ti in the hot oxidation of chromium-rich Ni–Co cast superalloys is investigated. This content is selected to stabilize the strengthening TiC population in the alloy. Yet, how can titanium, present in this rather high quantity, behave in such chromia-forming alloys? different scenarios may be expected:

- Can the presence of titanium lead to the formation of single or mixed oxides in the external oxide scale (possibly disturbing the growth of chromia)?
- Can this element take part to the constitution of an interfacial oxide separating alloy and the chromia scale with good or bad influence of the adherence of the later (as the $CrTaO_4$ formation which occurs for tantalum-containing alloys[22])?
- Is internal oxidation the single oxidation mode for titanium as for hafnium in HfC-reinforced chromia-forming alloys[23]?
- If the carbides network is composed of a great part of TiC, have these ones a tendency to disappear from the oxidation front to develop a carbide-free zone as TaC[22]? Or not as HfC[23]?

These questions will be explored by elaborating a series of six alloys based on nickel and cobalt in relative proportions regularly distributed and by characterizing the corresponding oxidized samples after a relatively long exposure in air (about a week) at a particularly high temperature (1200 °C) to enhance the influence of titanium.

II. EXPERIMENTAL

The chemical compositions of the alloys elaborated for this study are presented in Table I. All of them contain the same contents in chromium (25 wt pct) and carbon (0.4 wt pct). These two elements are very common in conventionally cast superalloys based on cobalt and nickel. They also contain all 1.6 wt pct Ti as element able to form monocarbides. Titanium chosen as MC-former element is more original than tantalum. To clearly distinguish these alloys from one another as well as from TaC-reinforced superalloys, a particular system of designation was chosen: ''nCo–b(5-*n*)Ni–Ti'' with ''n'' (respectively ''5-*n*'') equal to the number of fifths of Co (respectively Ni) in the base element position (proportions in mass fractions), and ''Ti'' as potential MC-former element. There are six alloys considered in this work: three Ni-richest alloys (from the cobalt-free ''0Co5NiTi'' alloy to the ''2Co3NiTi'' alloy) and three Co-richest alloys (from the ''3Co2NiTi'' alloy to the nickel-free ''5Co0NiTi'' alloy). The mixtures to melt for obtaining these alloys were composed of pure elements (Alfa Aesar, more than 99.9 wt pct for their purity). Each of these elements was cast using high frequency induction melting in inert atmosphere (CELES furnace operating at up to 5,000 Volts at 100,000 to 110,000 Hertz, fusion chamber closed by a water-cooled copper crucible and a silica tube, 0.3 bar of pure Ar)). Melting was achieved two times successively to be sure to be free of not-molten parts.

Table I. Designation and Chemical Compositions of the Studied Alloys

Wt Pct	M	Cr	Ti	C
0Co5NiTi	0*	25	1.6	0.4
1Co4NiTi	15*	25	1.6	0.4
2Co3NiTi	29*	25	1.6	0.4
3Co2NiTi	29**	25	1.6	0.4
4Co1NiTi	15**	25	1.6	0.4
5Co0NiTi	0**	25	1.6	0.4

*: Co, **: Ni.

The obtained ingots, each weighing 40 grams and presenting an ovoid shape, were cut using a metallography saw to obtain parts for the examination of the as-cast microstructures and parts for the exposures to laboratory air at high temperature. The parts for preliminary metallography were embedded in a mixture of Araldite resin and hardener (ESCIL). After total rigidification and extraction out of the plastic molds, the embedded samples were ground then polished with SiC papers and micrometric alumina-enriched textile disks, in order to obtain mirror-like samples for observations.

The rest of the ingot was cut in two halves which were ground until the 1200-grade of SiC paper, on the two main faces, with smoothing of the edges to avoid local overoxidation. These samples were each placed in an alumina shuttle. The six shuttles each containing one of the six alloys were put in the hot zone of a muffle resistive furnace. Here they were heated up to 1200 °C. After 170 hours of exposure to laboratory air at this temperature, the furnace was shut off and the oxidized samples cooled in the furnace still closed.

The part of external oxides which spalled off during cooling and remaining in the ceramic shuttles were collected and analyzed by X-ray diffraction (XRD). The oxides remaining on the surfaces of the oxidized samples were observed and analyzed by Energy Dispersion Spectrometry (EDS) on cross-sectional metallographic preparations. The as-cast and aged bulk microstructures of the alloys before and after oxidation test, the oxides still stuck on surface and the oxidation-induced microstructure changes in subsurface, were observed using a Scanning Electron Microscope JSM 6010 LA from JEOL. Spot analyses were carried out with the EDS device equipping the SEM to identify the external and internal oxides, to specify the chemical composition

in the outermost part of the alloys, and to obtain the concentration profiles of chromium and titanium between the oxidation front and the bulk.

III. RESULTS

A. *Microstructures of the Obtained Alloys*

The as-cast microstructures of the six alloys are illustrated in Figure 1 by SEM micrographs taken in Back Scattered Electrons mode (BSE). There are three common microstructural characteristics between these alloys: a polycrystalline equi-axed matrix, interdendritic carbides forming a eutectic with matrix, and a microstructure fineness characterized by about 25 μm for the secondary dendrite arm spacing. In contrast, the nature of the carbides varies from the cobalt-free nickel-based 0Co5NiTi alloy (only acicular chromium carbides) and the nickel-free cobalt-based 5Co0NiTi alloy (only script-like titanium carbides).

B. *Oxidized States Examination and Characterization Prior to Cutting*

A quarter of each ingot was exposed to laboratory air for 170 hours at 1200 °C. After cooling to room temperature these samples were more or less covered by external oxide scales and surrounded by oxides detached from their surfaces. The states of the oxidized surfaces of the two flat faces are shown in macrophotographs present in Figure 2. The oxides collected all around each sample (in the alumina shuttles) were subjected to X-ray diffraction (two of the obtained XRD diffractograms are given in Figures 3 and 4).

Obviously, spallation took place differently between the nickel-richest alloys (two top lines of macrographs in Figure 2) and the cobalt-richest ones (two bottom lines of macrographs in Figure 2). The 0Co5NiTi, 1Co4NiTi and 2Co3NiTi alloys were here and there totally denuded because of the local loss of all the thickness of external oxide (bright areas). The 3Co2NiTi, 4Co1NiTi and 5Co0NiTi alloys are still wholly covered by dark gray oxide but the external aspect of the scales is not homogenous (smooth or rough), and the thickness seems also to be different between areas on a same sample. In addition, these last samples were surrounded by oxides having obviously lost their surfaces.

The oxides lost by each sample were collected separately and XRD runs were carried out to determine their nature. Two examples of the obtained diffractograms are given in Figure 3 (oxides collected around one of the Ni-richest alloys) and in Figure 4 (oxides

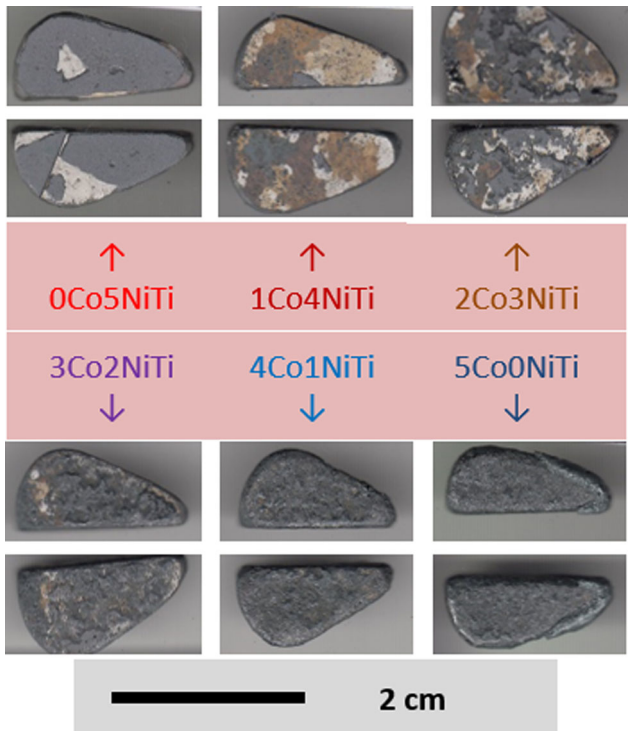

Fig. 2—Photographs of the two main faces of the six samples after oxidation.

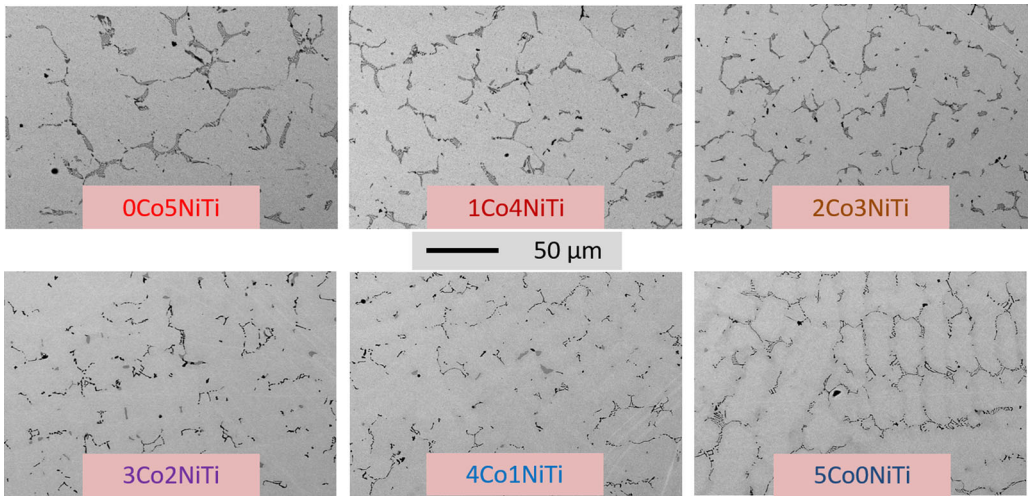

Fig. 1—SEM/BSE micrographs illustrating the microstructures of the alloys in their as-cast state (×500).

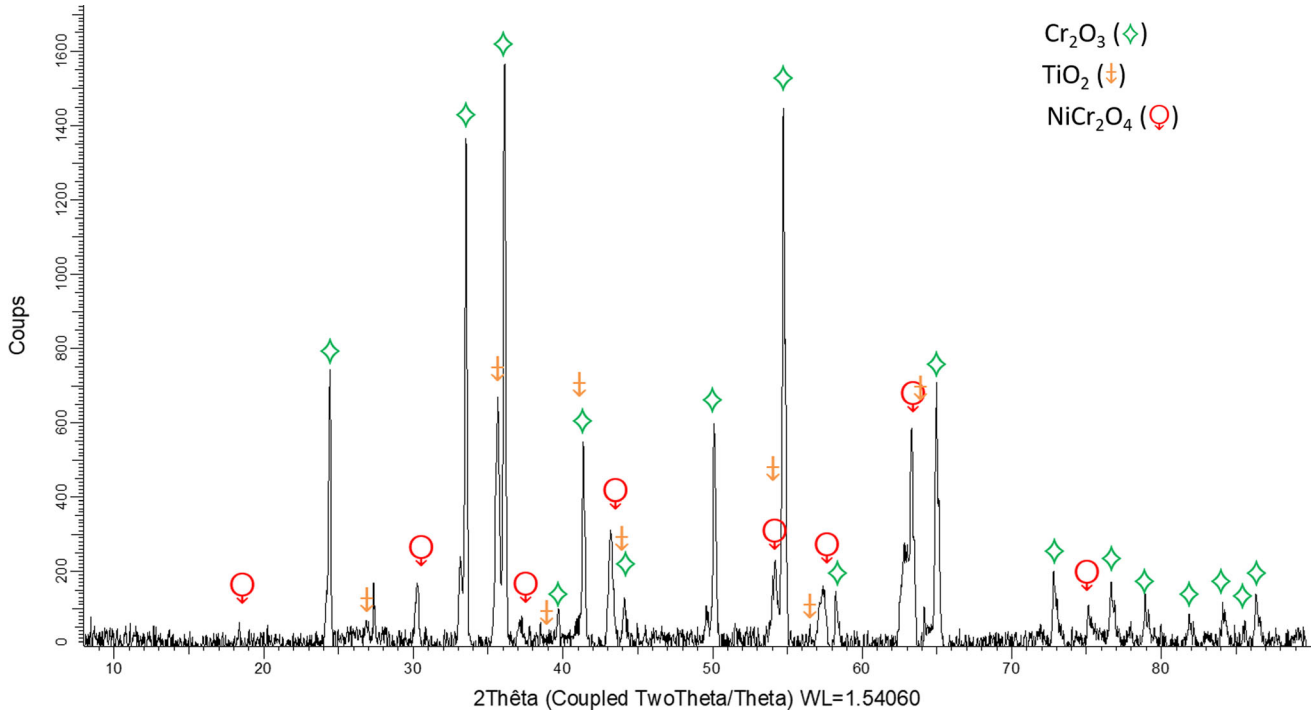

Fig. 3—Example of XRD pattern: here the oxidized surface of the 1Co4NiTi alloy.

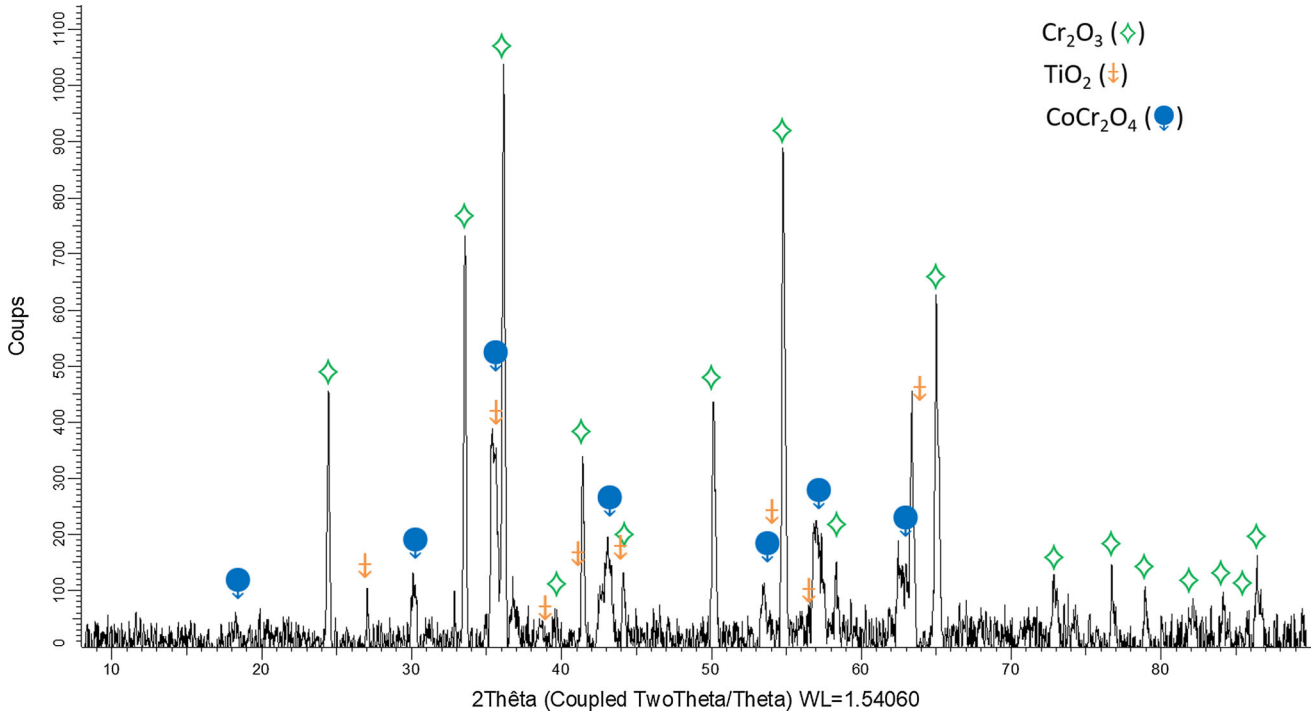

Fig. 4—Example of XRD pattern: here the oxidized surface of the 4Co1NiTi alloy.

collected around one of the Co-richest alloys). The whole obtained results are presented together in Table II. XRD allowed evidencing that two oxides formed on all the samples: chromia (Cr_2O_3) and titanium dioxide (TiO_2). Spinel oxides also formed for the alloys the cobalt content of which becomes equal to—or higher than—15 wt pct. Indeed, one notices the presence of $NiCr_2O_4$ or $(Ni,Co)Cr_2O_4$ for the

cobalt-containing Ni-richest alloys, and $CoCr_2O_4$ for the Co-richest alloys.

C. *Cross-Sectional Examination and Qualitative Characterization of the Oxidized States*

After embedding, transversal cutting, grinding and polishing the oxidized samples, their surfaces and subsurfaces were observed in cross-section (Figures 5 and 6). The different types of oxides still stuck on surface and the internal oxides were identified by EDS spot analysis (Figure 6, Table III).

In the cross-section, the external oxide scale appears to be mainly composed of chromia which obviously developed as a thick layer in contact with the metallic substrate. A continuous layer of titanium oxide has formed too, above chromia (*i.e.* separating chromia from air during the high temperature exposure). During cooling, the outermost oxide TiO_2 has been lost here and there without or with the corresponding part of chromia. In the case of the alloys which are the richest in cobalt, shear rupture obviously occurred and the inner part of the chromia scale remained stuck on the alloy while the outer chromia and the outermost TiO_2 scale quitted the samples. For these later Co-rich alloys, one also notices a start of inward progress of oxidation, revealed by an irregular oxide/alloy frontier and, in some locations, a deep penetration of oxidation. For the same Co-richest alloys, the presence of thick $CoCr_2O_4$ mixed with CoO oxides suggests that generalized oxidation was taking place in these locations.

In the subsurface, one can observe a more or less deep disappearance of carbides (chromium carbides and/or titanium carbides) as well as an internal oxidation progress. Many internal oxides are made of chromia, but most often this is $TiCr_2O_4$ which is encountered (identified by spot EDS analysis, example of approximative measured composition: 11 Ti–32 Cr–57 O, in at. pct). In addition, many porosities also formed. The list of the oxides observed in cross-section in the external oxide scales and in the subsurface are recapitulated in Table III. By comparison, with Table II, one can see that the most part of the spinel oxides was lost with the oxide scales spalled off during cooling while the $TiCr_2O_4$ oxides were logically kept in the alloys since they formed essentially internally.

D. *Quantitative Characterization of the Oxidized States*

Several parameters characterizing the oxidation products or the degradation caused by oxidation to the alloys were subjected to measurements. The thickness of the chromia scale is plotted in Figure 7 together with the one of the outermost TiO_2 scale (five values per alloy).

Table II. Oxides (Other than Cr_2O_3 and TiO_2 Which Are Both Present for All Alloys) Identified by XRD Among the Scales Spalled Off During Cooling and Collected in the Ceramic Shuttles

XRD Peaks	Oxides (Other Than Chromia and Titanium Di-Oxide)
0Co5NiTi	—
1Co4NiTi	$NiCr_2O_4$
2Co3NiTi	$(Co,Ni)Cr_2O_4$
3Co2NiTi	$CoCr_2O_4$
4Co1NiTi	$CoCr_2O_4$
5Co0NiTi	$CoCr_2O_4$

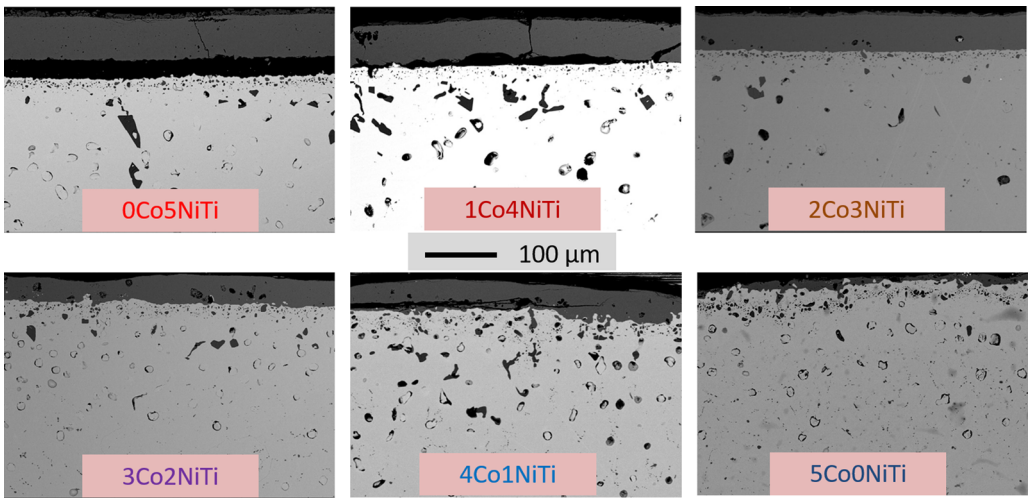

Fig. 5—SEM/BSE micrographs illustrating the surface states of the oxidized alloys (×250).

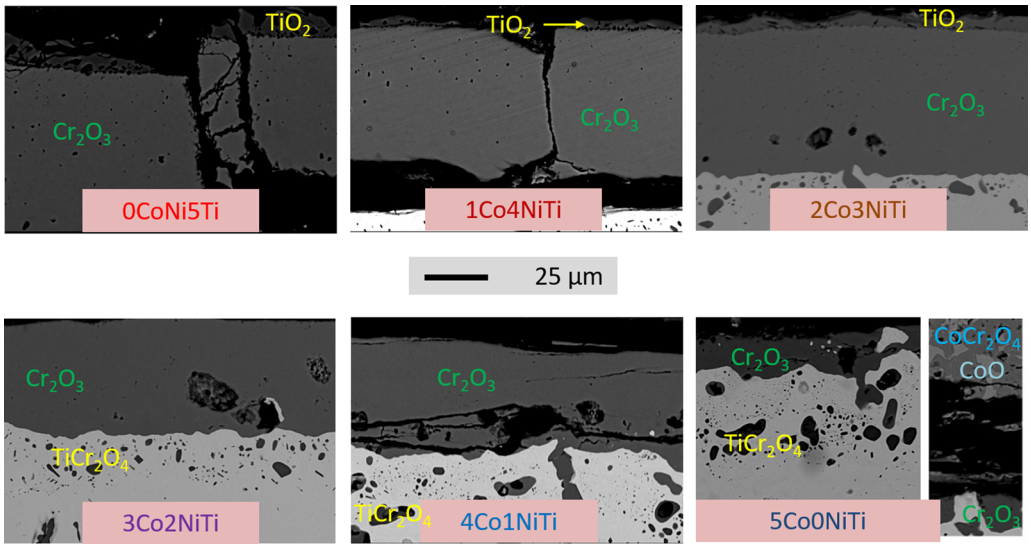

Fig. 6—SEM/BSE micrographs illustrating the surface states of the oxidized alloys (×1000).

The chromia scale was particularly preserved from spallation for the cobalt-free alloy (0Co5NiTi): the thickness is the greatest and the scale is regular. The average value decreases when Co is present in the alloy while the standard deviation increases significantly. This reveals the loss of a part of thickness by shear rupture during cooling: this oxide loss seems limited for the alloys with rather equilibrated contents in Co and Ni, but greater for the two Co-richest alloys (4Co1NiTi and 5Co0NiTi). The TiO_2 thickness follows the same trend. Each time the outer part of chromia was lost the corresponding outermost TiO_2 was lost too. The average TiO_2 thickness is maximal for the 0Co5NiTi alloy, lower for the 1CoNiTi and 2Co3NiTi alloys, and the external TiO_2 was lost everywhere for the cobalt-richest alloys.

After the external oxides, the distribution of the two principal types of internal oxides was also characterized, by measuring the depth of existence of these internal oxides from the scale/alloy interface (five values per alloy). Results are plotted together in Figure 8. The depth of appearance of the oxides involving chromia (internal Cr_2O_3 and $TiCr_2O_4$) is obviously maximal for the two Ni-richest alloys ($\approx$ 30 to 70 μm) and lower for the four other alloys ($\approx$ 20 to 25 μm). Seemingly TiO_2 formed significantly deeper for the two Ni-richest alloys ($\approx$ 125 μm) than for the four other alloys ($\approx$ 80 μm).

Another consequence of oxidation for the subsurface is the disappearance of carbides. The depth of carbide disappearance, again counted from the oxide scale/alloy interface, was measured (five values per alloy) for the two types of carbides (chromium carbides and titanium carbides). The depth of carbide disappearance decreases with the increase in cobalt in the alloy. One can remark that the disappearance of the chromium carbides is twice than that of the TiC carbides. For the 0Co5NiTi alloy which contains only chromium carbides there is no depth of TiC disappearance, logically. Similarly, for the two Co-richest alloys which did not contain chromium carbides, only the TiC disappearance depth has some signification (Figure 9).

A series of chemical measurements were carried out in extreme surface of the alloys (metallic part just under the oxide/alloy interface) and in the subsurface. The EDS spot analyses performed in the alloy very close to the {oxide scale/alloy} interface led to the obtained contents in chromium and tantalum which are graphically presented in Figure 10. Due to oxidation, the local chromium content has decreased down to values equal to 16 wt pct Cr for the Ni-richest alloy, and to lower values for the other alloys. Indeed the Cr content in the outermost part of alloy decreases progressively with the presence of more and more cobalt, from the 16 wt pct for the 0Co5NiTi alloy to slightly lower than 15 wt pct for the 5Co0NiTi alloy. At the same time the titanium content varies too, but with no systematic trend.

Some concentration profiles were acquired inwards, from the {oxide scale/alloy} interface. They are shown in Figure 11 for chromium and in Figure 12 for titanium. One finds again the slight decrease in chromium content in extreme surface when the alloy contains more and more cobalt. These profiles additionally show that the chromium-depleted zone is not really different between the six alloys (about 300 μm for all of them), but the maximal concentration gradients in chromium (linear parts over the first 200 μm from the {oxide scale/alloy} interface) are seemingly higher for the Co-richest alloys than for the Ni-richest ones. The titanium concentration profiles are much more irregular, perturbed by the presence of a dense population of titanium oxides. This does not allow comparing them to one another efficiently. Seemingly there is no correspondence between the depths of the carbide-free zones, neither with the chromium-depleted depths, nor with the high Cr gradient parts in the concentration profiles.

Table III. Identification by EDS of the Oxides Remaining on Surface and Observed on Cross-Sections

Spot EDS	Internal Oxides	External Oxides
0Co5NiTi	TiO_2, $TiCr_2O_4$, Cr_2O_3	Cr_2O_3, TiO_2
1Co4NiTi		
2Co3NiTi		
3Co2NiTi		
4Co1NiTi		
5Co0NiTi	TiO_2, $TiCr_2O_4$, Cr_2O_3	Cr_2O_3, TiO_2, $CoCr_2O_4$, CoO

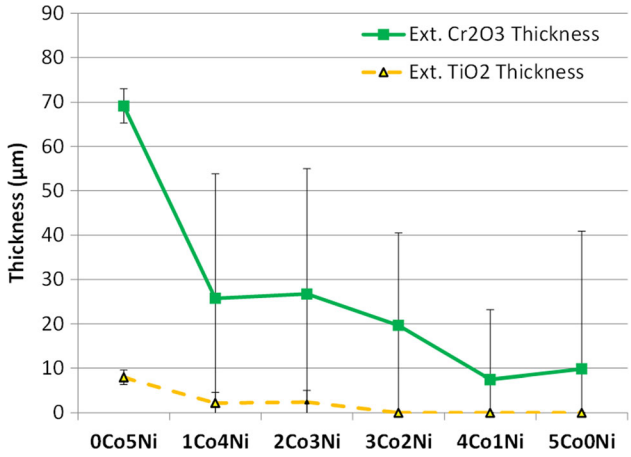

Fig. 7—Thicknesses of the two main oxides of the continuous external scale: Cr_2O_3 and TiO_2 (outermost oxide).

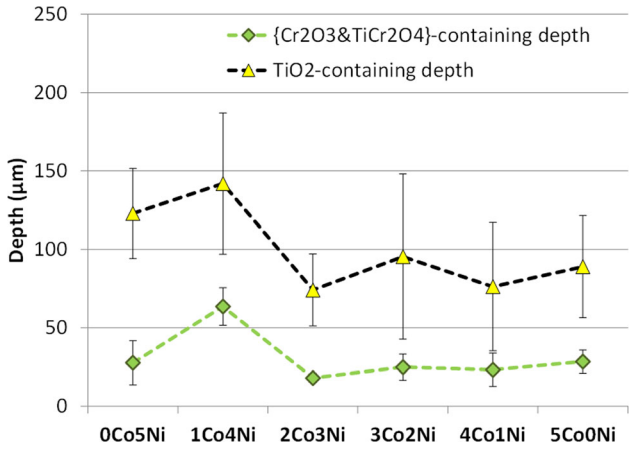

Fig. 8—Depth of presence of internal $Cr_2O_3/TiCr_2O_4$ and TiO_2 in the subsurface.

E. *Evolution of the Microstructure in the Bulk*

The potential evolution of the microstructure at the core was also investigated by SEM. The initial microstructures of the three Ni-richest alloys are reminded, with a higher magnification than in Figure 1, in the top part of Figure 13 and in the top part of Figure 14 for the three Co-richest alloys. In the bottom parts of these figures the corresponding SEM micrographs, taken in the bulk of the alloys after exposure at 1200 °C for 170 hours, evidence the

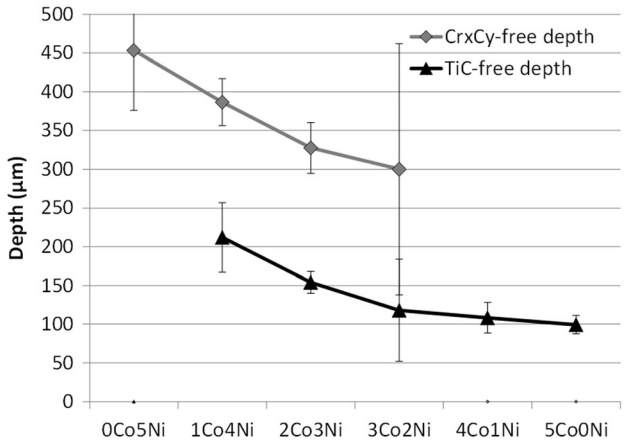

Fig. 9—Depths of disappearance of chromium carbides and titanium carbides.

morphological evolution of the carbides. The chromium carbides (medium gray), which were finely structured (acicular-shaped) have considerably coarsened. The titanium carbides have themselves significantly changed; they become very round too.

IV. DISCUSSION

Obviously, the addition of titanium to {Ni, Co}–25 wt pct Cr–0.4 wt pct C alloys did not lead systematically to the formation of titanium carbides during solidification. However titanium is known as a strong carbide-former metal and TiC are among the most stable carbides.[24] In most of the alloys of the present work titanium undergoes competition with chromium. In their as-cast states, this led to the simultaneous presence of chromium carbides and titanium carbides in the three medium alloys containing 29 wt pct Co and more (from 2Co3NiTi to 4Co1NiTi). For 15 wt pct Co and less (1Co4NiTi and 0Co5NiTi) chromium carbides are nearly the single carbide phase present. TiC carbides are alone only in the nickel-free Co-based alloy 5Co0NiTi. The very greatest part of cast superalloys earlier studied and containing simultaneous titanium and carbon in proportions potentially leading to MC carbides are based on nickel while results are lacking concerning cast alloys based on cobalt and containing these two elements simultaneously. In chromium-containing cast Ni-based alloys TiC carbides are almost

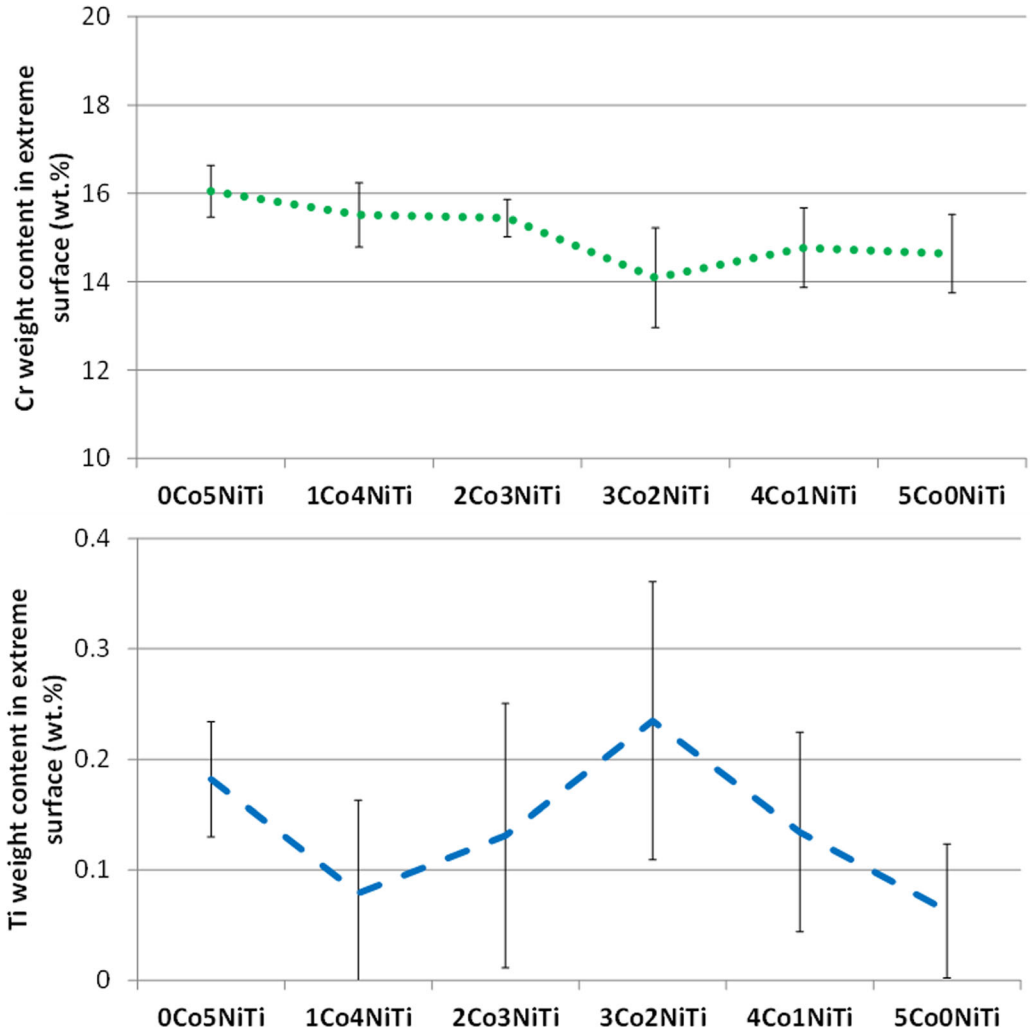

Fig. 10—Chromium (top) and titanium (bottom) contents in the outermost part of the alloys.

never present since these alloys—often commercial—generally contain other MC-former elements at the same time, often niobium and sometimes molybdenum and tungsten, and rarely tantalum, hafnium. In these alloys MC carbides involving titanium may be obtained as single carbide present[25] or as carbide co-existing with chromium-rich $M_{23}C_6$ carbides.[26] In some cases, despite the presence of Ti and C in significant quantities, no MC carbides, thus no carbide involving titanium, are present.[27,28] In the model alloys of the present study, MC carbides involving titanium must be necessarily TiC and, without the help of the presence of niobium for instance, no TiC formed in the two Ni-richest alloys and the single carbides to form were chromium carbides. In addition, the chromium contents in the present alloys (25 wt pct Cr) are significantly higher than the {Ti, C}-containing Ni-based alloys earlier studied in the literature (more or less 15 wt pct Cr), and this favored chromium carbides here.

Another particularity of the model alloys of the present study is the presence of cobalt as alloying element and even base element. For the concerned alloys, in absence of niobium and other MC-former element than Ti, this obviously helped the formation of TiC carbides, an effect never reported in previous studies to the best of our knowledge. The carbon contents rather high (0.4 wt pct C) when compared with earlier studied MC-containing (M = Ti and other elements) alloys, led to significant fractions of TiC carbides. It was earlier reported that the higher the carbon content, the greater the fraction of Ti-involving MC carbides,[29] with as consequence an enhanced creep-resistance.[30]

The alloys of this study in which TiC formed in significant quantities (the cobalt-richest alloys) contains script - like TiC carbides, a morphology which allows improving the interdendritic cohesion. This was not really the case of the previous alloys containing MC carbides involving titanium since they were frequently elongated or blocky and even spheroidal carbides,[11,31] and sometimes inter-grains carbides films.[32]

The carbides had morphologically evolved but their natures and proportions were the same at the end of the long exposures at elevated temperatures resulting from the oxidation tests. They became blocky and coarsened, a phenomenon which was earlier reported in the case of the Ti-containing MC carbides initially formed in

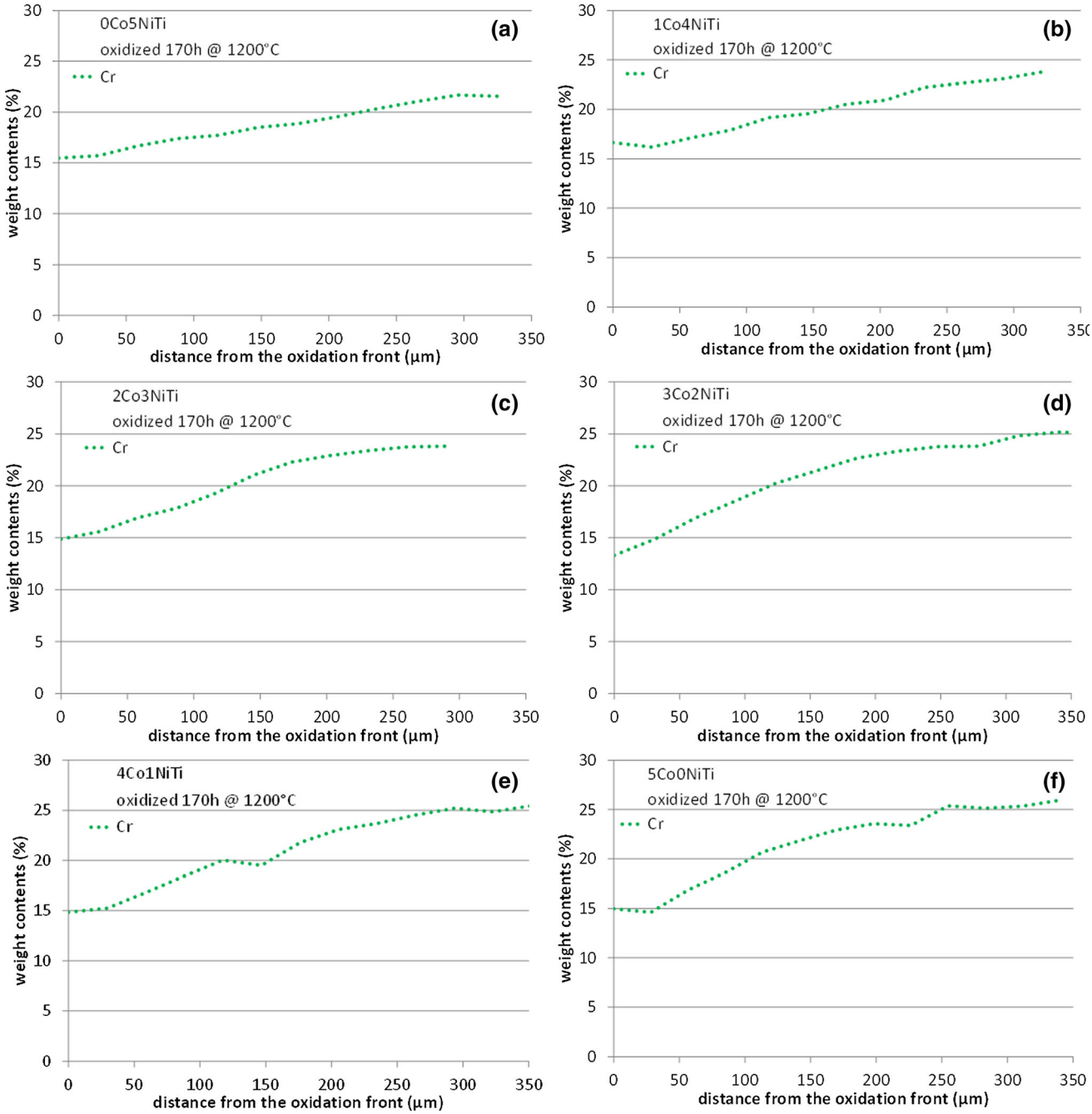

Fig. 11—Concentrations profiles in chromium from the oxide scale/alloy interface (SEM/EDS); (*a*) 0Co5NiTi, (*b*) 1Co4NiTi, (*c*) 2Co3NiTi, (*d*) 3Co2NiTi, (*e*) 4Co1NiTi, (*f*) 5Co0NiTi.

previously alloys.[32,33] This showed that the double population of chromium carbides and titanium carbides did not result from non-equilibrium crystallization but corresponds to the metallurgical state stable at this temperature. In contrast the particularly complex morphology of both carbides (TiC and chromium carbides), governed by the growth mechanisms at solidification, and which created a high interfacial energy, led to this loss of the script-like (TiC) or acicular (chromium carbide) morphology and to subsequent coarsening, that usually occurs and was noticed in earlier works.

Concerning their behaviors in oxidation, one can say that the alloys rather well resisted, taking into account the long time of exposure to air and the high level of temperature. The main chemical parameter governing the level of hot oxidation resistance was not really titanium but the relative proportions of nickel and cobalt in the alloys: external chromia for the nickel-rich alloys, and chromia added with significant quantities of $CoCr_2O_4$ spinel, and even CoO for the alloys richest in cobalt, notably free of nickel (5Co0NiTi alloy). NiO and $NiCr_2O_4$ were also detected for the Ni-rich alloys, but in much lower quantities. Cobalt or cobalt-chromium

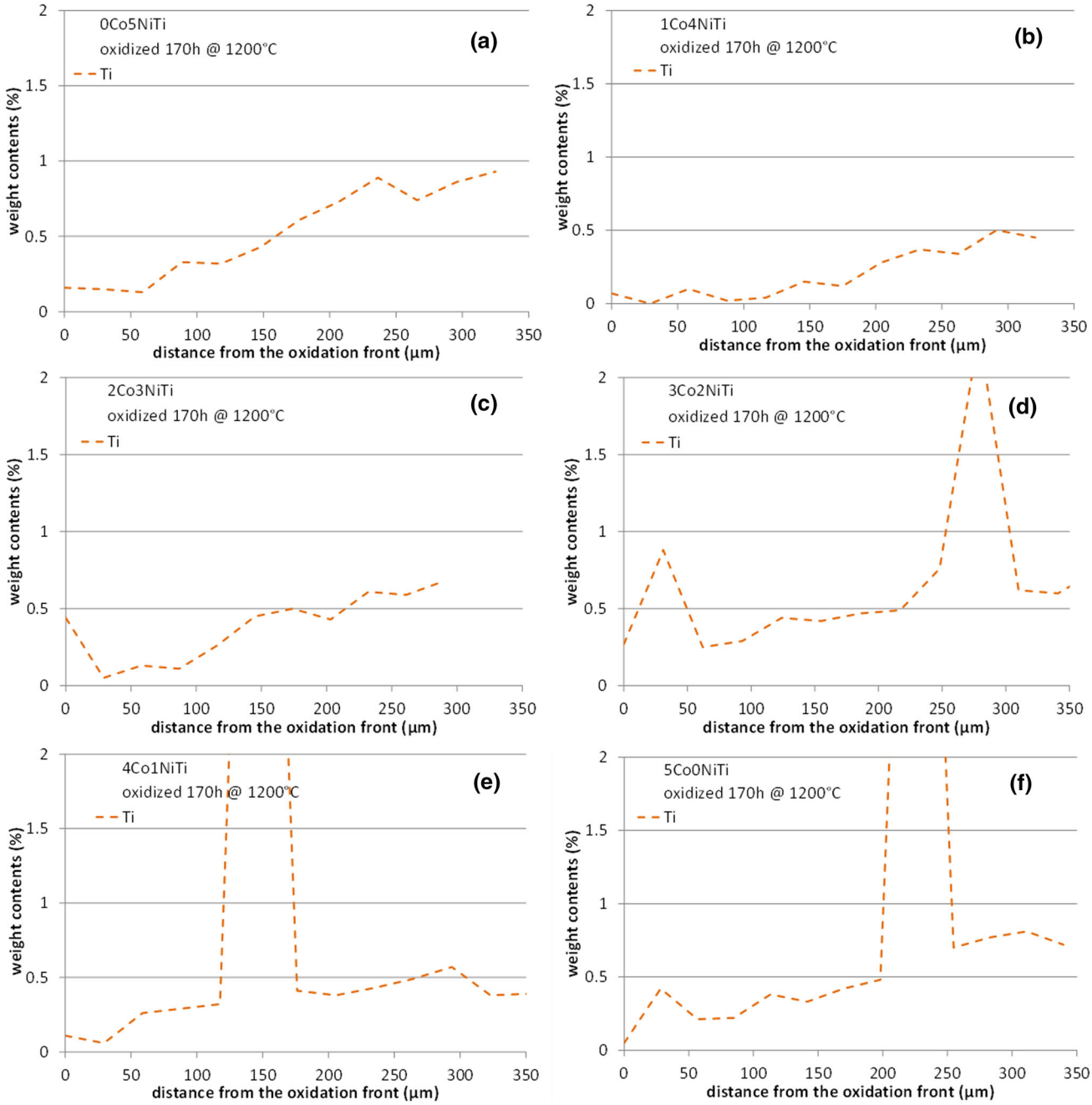

Fig. 12—Concentrations profiles in titanium from the oxide scale/alloy interface (SEM/EDS); (*a*) 0Co5NiTi, (*b*) 1Co4NiTi, (*c*) 2Co3NiTi, (*d*) 3Co2NiTi, (*e*) 4Co1NiTi, (*f*) 5Co0NiTi.

oxides formed in the case of the cobalt-richest alloys, suggesting the start of generalized oxidation with an inward progression. This is the lack of easiness of chromium volume diffusion through the matrix, due to the predominance of cobalt over nickel, which is at the origin of this deteriorated oxidation behavior by comparison the one of the nickel-richest alloys. The insufficient chromium supply of the oxidation front made possible the diffusion of some O^{2-} anions up to meeting with chromium and the metals other than Cr in the subsurface. These were the main difference of oxidation behavior between these two groups of alloys.

Furthermore, it was easily observed that the alloys richest in nickel developed only a double external oxide scale, composed of a thick continuous chromia scale in contact with the alloy substrate, topped with a thin continuous TiO_2 layer isolating chromia from hot air. This double constitution of the external oxide scale, which was clearly seen here when the scale remained on the alloy despite the tendency to spallation during cooling, was earlier observed in other oxidized superalloys containing titanium.[34–36] Whatever it happened during cooling, collecting the lost oxides and analyzing them with the X-ray diffractometer allowed seeing that

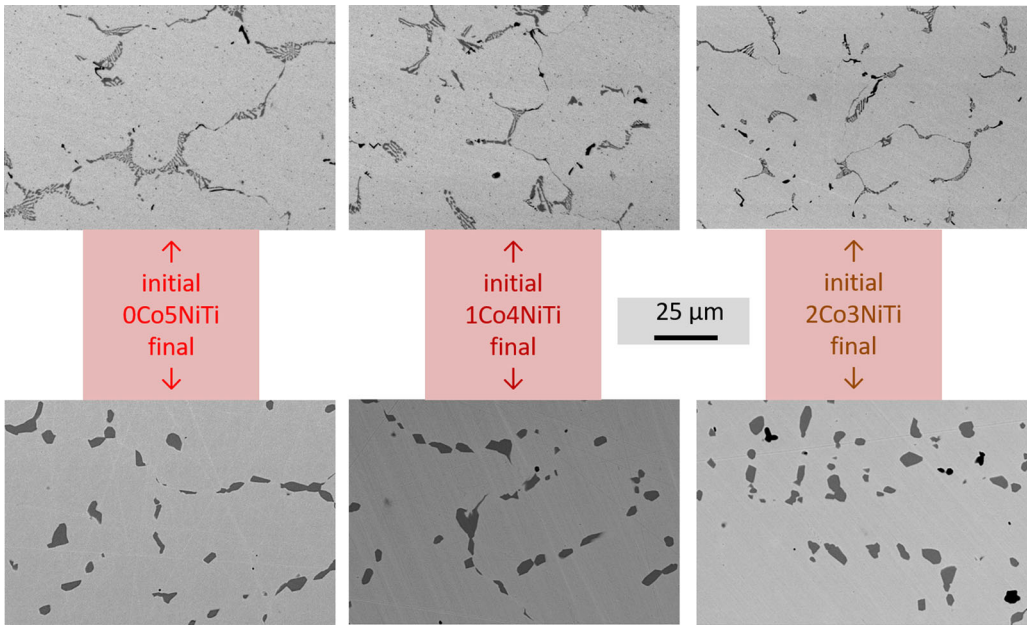

Fig. 13—SEM/BSE micrographs illustrating the initial and final microstructures in the bulk of the three Ni-richest alloys (×1000).

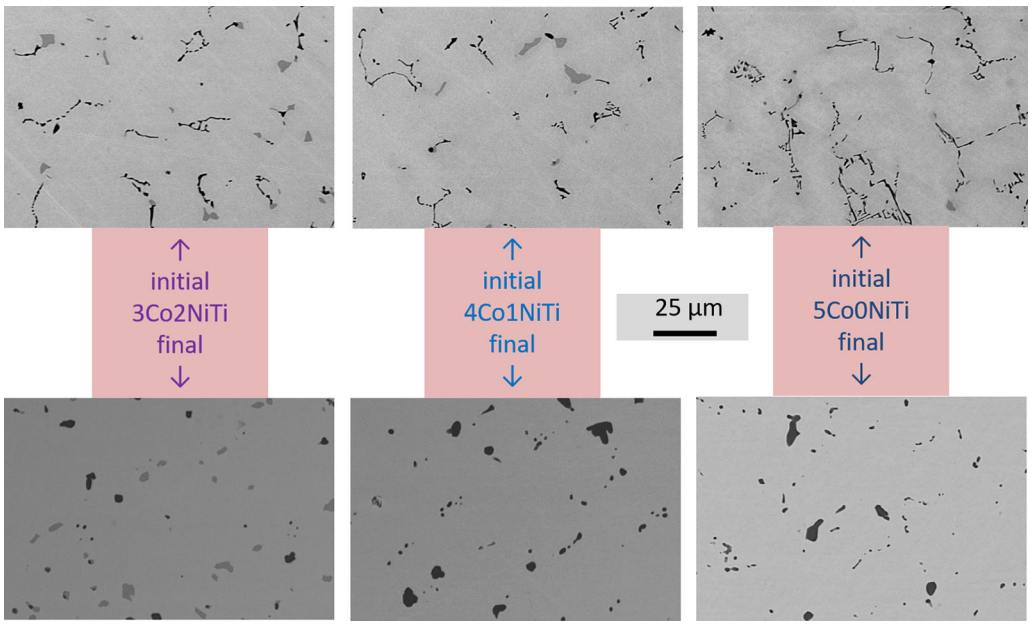

Fig. 14—SEM/BSE micrographs illustrating the initial and final microstructures in the bulk of the three Co-richest alloys (×1000).

TiO_2 was present in the external scale even for the alloys richer in cobalt than in nickel, despite the tendency of the latter ones to lose their outermost part of external oxide by shear rupture. The external TiO_2 layer tended to be thicker for the nickel-richest alloys: this suggests an easier outwards diffusion of titanium, which can be explained by the easy availability of the Ti atoms only present in solid solution in the matrix. If it is clear that Ti really diffused outwards for all alloys (demonstrated by the gradient existing in all the Ti concentrations profiles), oxygen also entered the alloys and diffused inwards, inducing internal oxidation as previously noticed in the subsurface of titanium-containing superalloys.[37,38] Oxygen met easier Ti (and Cr) to form internal TiO_2 and $TiCr_2O_4$ in their subsurfaces in the case of the nickel-richest alloys than in the cobalt-richest alloys, since Ti was more available in solid solution in the former alloys than in the later ones. This resulted in more extended internal oxidation involving Ti for the nickel-richest alloys than for the cobalt-richest ones, as observed in cross-section.

Concerning again the outward Ti diffusion during oxidation of the nickel-richest alloys, this destabilized the not many TiC existing in the ones of these alloys

which contained some cobalt, and the depth of disappearance of TiC was particularly important by comparison with the cobalt-richest alloys containing more TiC carbides and less Ti in solid solution consequently. However this ought to have no real impact on the mechanical properties of the alloys since these depths are low in all cases. What is much worrisome is the considerable change in morphology carbides resulting from the long exposure at elevated temperature for all the alloys: coarsening and almost spheroidization of the TiC as well as of the chromium carbides, with the loss of their Chinese script morphology for the formers and of their acicular shapes for the later. High temperature mechanical tests carried out on as-cast alloys and on their aged versions and the comparison of their results will teach us what can be the consequences of these morphology changes of these hardening particles.

V. CONCLUSION

Titanium initially added to help forming MC carbides did not succeed in obtaining titanium carbides in the nickel-richest alloys, in contrast with the more complex alloys earlier studied in which other elements—such as niobium—which certainly helped the MC formation, but the TiC formation successfully occurred in the cobalt—richest alloys. Unfortunately, at 1200 °C, these carbides seemed being really morphologically not stable, with the loss of their script-like morphology before the end of the 170 hours tested here. The addition, beside titanium, of small amounts of other MC-former elements (Nb for instance) may improve this morphological behavior—as well as the MC formation even in the nickel-richest alloys. This will be tested in a new work.

Concerning the behavior in hot oxidation, all the questions asked in the introduction are now answered. The presence of titanium induces the formation of new oxides—TiO_2 or $TiCr_2O_4$—in addition to chromia which remained the principal external oxide scale. The general oxidation behavior is not influenced by these oxides and the differences of oxidation resistance is still governed by the base element. Furthermore, depending on this base element of the alloy, these titanium single or mixed oxides formed externally (TiO_2, Ni-richest alloys) or internally ($TiCr_2O_4$, Co-richest alloys), but never at the interface between the alloy surface and the chromia scale. No deleterious influence of titanium on the scale adherence is thus expected, in contrast with what may occur for the tantalum-containing alloys. Concerning the carbide disappearance in subsurface due to oxidation—earlier observed for the alloys containing TaC carbides—it effectively occurred for the TiC carbides, but only for the cobalt-richest alloys which were the only ones here to contain titanium carbides.

The not really expected additional phenomenon which took place because of the presence of titanium is the development of the thin but continuous outermost layer isolating chromia from oxidizing air. This may be favorable to the long term sustainability of the alloys: by isolating chromia from the oxidant atmosphere, it can possibly limit the re-oxidation of chromia in gaseous species—phenomenon particularly active at so high temperature—and then the chromium consumption. This possible beneficial effect will be verified by oxidation tests including thermogravimetric measurements to assess chromia volatilization rates and compare the ones for Ti-free alloys and for the same alloys added with titanium.

ACKNOWLEDGMENTS

The authors wish to thank Mr. Lionel Aranda and Ghouti Medjahdi for their technical help.

CONFLICT OF INTEREST

On behalf of all authors, the corresponding author states that there is no conflict of interest.

REFERENCES

1. C.T. Sims and W.C. Hagel: *The Superalloys*, Wiley, New York, 1972.
2. E.F. Bradley: *Superalloys: A Technical Guide*, ASM International, Metals Park, 1988.
3. P. Kofstad: *High Temperature Corrosion*, Elsevier Applied Science, London, 1988.
4. D.J. Young: *High Temperature Oxidation and Corrosion of Metals*, Elsevier, Amsterdam, 2008.
5. M.J. Donachie and S.J. Donachie: *Superalloys—A Technical Guide*, 2nd ed., ASM International, Materials Park, 2002.
6. J. Chen, Q. Huo, J. Chen, Y. Wu, Q. Li, C. Xiao, and X. Hui: *Mater. Sci. Eng. A.*, 2021, vol. 799, art. no. 140163.
7. L. Ouyang, R. Luo, Y. Gui, Y. Cao, L. Chen, Y. Cui, H. Bian, K. Aoyagi, K. Yamanaka, and A. Chiba: *Mater. Sci. Eng. A.*, 2020, vol. 788, art. no. 139638.
8. P. Zhou, X. Gao, D. Song, Q. Liu, Y. Liu, and J. Cheng: *J. Mater. Res.*, 2020, vol. 35, pp. 2737–45.
9. Y. Zhai, L. Yang, F. Xue, Y. Chen, and S. Mao: *Crystals*, 2020, vol. 10, art. no. 908.
10. Y.L. Ge and J.Y. Wang: *Prakt. Metallogr.*, 1983, vol. 20, pp. 554–61.
11. X.Z. Qin, J.T. Guo, C. Yuan, J.S. Hou, and H.Q. Ye: *Mater. Lett.*, 2008, vol. 62, pp. 2275–78.
12. A. Baldan and J.M. Benson: *Z. Metall.*, 1990, vol. 81, pp. 446–51.
13. Z. Yu, L. Liu, X. Zhao, W. Zhang, J. Zhang, and H. Fu: *Trans. Nonferrous Met. Soc. China*, 2010, vol. 20, pp. 1835–40.
14. S. Skolianos, T.Z. Kattamis, M. Chen, and B.V. Chambers: *Mater. Sci. Eng. A*, 1994, vol. 183, pp. 195–204.
15. B. Zheng, T. Topping, J.E. Smugeresky, Y. Zhou, A. Biswas, D. Baker, and E.J. Lavernia: *Metall. Mater. Trans. A*, 2010, vol. 41A, pp. 568–73.
16. M. Khair and P. Berthod: *Calphad*, 2019, vol. 65, pp. 34–41.
17. J.L. Walter and H.E. Cline: *Metall. Trans.*, 1973, vol. 4A, pp. 1775–84.
18. D.A. Woodford: *Metall. Trans. A*, 1977, vol. 8A, pp. 2016–2019.
19. P. Berthod, S. Michon, L. Aranda, S. Mathieu, and J.C. Gachon: *Calphad*, 2003, vol. 27, pp. 353–59.
20. I.L. Mogford and D. Hull: *J. Iron Steel Inst.*, 1968, vol. 206, pp. 79–84.
21. P. Berthod, Y. Hamini, L. Aranda, and L. Héricher: *Calphad*, 2007, vol. 31, pp. 351–60.
22. P. Berthod, J.P. Gomis, and G. Medjahdi: *Metall. Mater. Trans. A*, 2020, vol. 51A, pp. 4168–85.
23. P. Berthod and E. Conrath: *Mater. High Temp.*, 2014, vol. 31, pp. 266–73.
24. S.R. Shatynski: *Oxid. Met.*, 1979, vol. 13, pp. 105–118.

25. F.S. Yin, X.F. Sun, J.G. Li, H.R. Guan, and Z.Q. Hu: *Mater. Lett.*, 2003, vol. 57, pp. 3377–80.
26. D.L. Shu, S.G. Tian, N. Tian, J. Xie, and Y. Su: *Mater. Sci. Eng. A*, 2017, vol. 700, pp. 152–61.
27. X.B. Hu, Y.L. Zhu, L.Z. Zhou, B. Wu, and X.L. Ma: *Philos. Mag. Lett.*, 2015, vol. 95, pp. 237–44.
28. X.B. Hu, X.Z. Qin, J.S. Hou, L.Z. Zhou, and X.L. Ma: *Philos. Mag. Lett.*, 2017, vol. 97, pp. 43–49.
29. S. Dodangeh, F. Shahri, and S.M. Abbasi: *High Temp. Mater. Proc.*, 2015, vol. 34, pp. 821–26.
30. W. Wang, R. Wang, A. Dong, G. Zhu, D. Wang, W. Zhou, W. Pan, D. Shu, and B. Sun: *Mater. Sci. Eng. A*, 2019, vol. 756, pp. 11–17.
31. P. Kontis, D.M. Collins, A.J. Wilkinson, R.C. Reed, D. Raabe, and B. Gault: *Scr. Mater.*, 2018, vol. 147, pp. 59–63.
32. W. Sun, X. Qin, J. Guo, L. Lou, and L. Zhou: *Mater. Des.*, 2015, vol. 69, pp. 81–88.
33. Q. Li, S. Tian, H. Yu, N. Tian, Y. Su, and Y. Li: *Mater. Sci. Eng. A*, 2015, vol. 633, pp. 20–27.
34. Y.-H. Lee, S. Ko, H. Park, D. Lee, S. Shin, I. Jo, S.-B. Lee, S.-K. Lee, Y. Kim, and S. Cho: *Appl. Surf. Sci.*, 2019, vol. 480, pp. 951–55.
35. H. Zhang, Y. Liu, X. Chen, H. Zhang, and Y. Li: *J. Alloys Compd.*, 2017, vol. 727, pp. 410–18.
36. X. Zhuang, Y. Tan, X. You, P. Li, L. Zhao, C. Cui, H. Zhang, and H. Cui: *Vacuum.*, 2021, vol. 189, art. no. 110219.
37. J. Cao, J. Zhang, R. Chen, Y. Ye, and Y. Hu: *Mater. Charact.*, 2016, vol. 118, pp. 122–28.
38. L. Chen, Y. Sun, L. Li, and X. Ren: *Corrs. Sci.*, 2020, vol. 169, art. no. 108606.